Supplementary Information

Influence of lattice oxygen on the catalytic activity of blue titania supported Pt catalysts under CO oxidation

Hanseul Choi,[ac] Jinsun Lee,[bd] Daeho Kim,[ac] Ashwani Kumar,[bd] Beomgyun Jeong,[e] Ki-Jeong Kim,[f] Hyoyoung Lee,[*bd] and Jeong Young Park[*ac]

[a]*Department of Chemistry, Korea Advanced Institute of Science and Technology (KAIST), Daejeon 34141, Republic of Korea*

[b]*Department of Chemistry, Sungkyunkwan University, Suwon 440-746, Republic of Korea*

[c]*Center for Nanomaterials and Chemical Reactions, Institute for Basic Science, Daejeon 34141, Republic of Korea*

[d]*Center for Integrated Nanostructure Physics, Institute for Basic Science, Sungkyunkwan University, Suwon 440-746, Republic of Korea*

[e]*Advanced Nano Surface Research Group, Korea Basic Science Institute (KBSI), Daejeon 34133, Republic of Korea*

[f]*Beamline Research Division, Pohang Accelerator Laboratory (PAL), Pohang 37673, Republic of Korea*

Supplementary notes

Supplementary note 1: EPR analysis

To measure the Ti^{3+} sites ($3d^1$, S = 1/2) and oxygen-based radicals, including oxygen anions and superoxide radical anions. EPR spectra was measured and shown in Figure S14. No EPR signal was measured with TiO_2 (P25). However, TiO_{2-x} showed two sets of EPR signal; low-field peak and high-field peak. The low-field feature could be assigned to oxygen species and the hole trapped in oxygen anions, and high-field component is assigned to electrons trapped at Ti^{3+} centers. The signal at g= 1.911 originated from vacancy-stabilized Ti^{3+}, and the signal at $g_{\parallel}$=1.962 , $g_{\perp}$=1.994 could be assigned to electrons trapped in localized states (Ti^{3+}) in the anatase phase[1-3]. A new signal at g=2.0102 appears with TiO_{2-x} and comes from a hole trapped at oxygen anions[4]. This is because, when the oxygen vacancies form in lattice, excess electrons can be generated, and the excess electrons are preferentially trapped in Ti^{4+} states to form Ti^{3+} states. Besides, the generated hole could be trapped in localized states (O^{2-}) to form oxygen anions[1]. The EPR results clearly support the formation of Ti^{3+} and oxygen vacancies.

Supplementary Tables

Table S1 Physical properties of TiO_2, and blue TiO_2 supports and Pt loaded on the supports.

	BET surface area (m^2/g)	**Pore volume (cm^3)**	**Pt loading (wt %)**
TiO_2	51.5	0.13	0.7
Blue TiO_2	54.0	0.40	0.7

Table S2 H_2-TPR results of Pt deposited on TiO_2 and blue TiO_2 catalysts.

Pt/TiO_2		**Pt/blue TiO_2**	
Temperature (°C)	H_2 consumption (10^{-3} mmol g^{-1})	Temperature (°C)	H_2 consumption (10^{-3} mmol g^{-1})
74.2	32.1	89.8	54.5
333.9	4.7	340.3	16.5
591.1	5.0	457.2	12.0

Table S3 Ratio of the lattice oxygen and the binding energy with Pt/TiO_2 and Pt/blue TiO_2 analyzed by XPS with Al Kα.

	Ti-O before reaction (%)	**Ti-O binding energy (before reaction) (eV)**	**Ti-O After reaction (%)**	**Ti-O binding energy (after reaction) (eV)**
Pt/TiO_2	69.1	529.8	40.7	529.9
Pt/blue TiO_2	65.2	529.5	30.5	529.9

Table S4 Ratio of the lattice oxygen of Pt/TiO_2 and Pt/Blue TiO_2 under UHV and during the CO oxidation reaction analyzed by NAP-XPS with 600 eV of *h*v.

	Ti-O (UHV, %)	**Ti - O (CO oxidation, %)**
Pt/TiO_2	53.7	10.2
Pt/Blue TiO_2	50.4	6.1

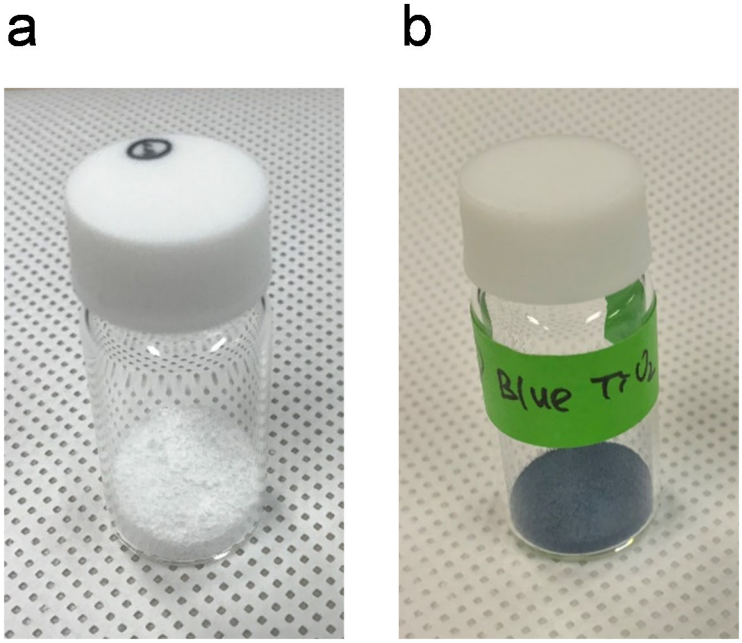

Fig. S1 (a) Photograph of TiO_2 (Degussa) and (b) as-synthesized blue TiO_2.

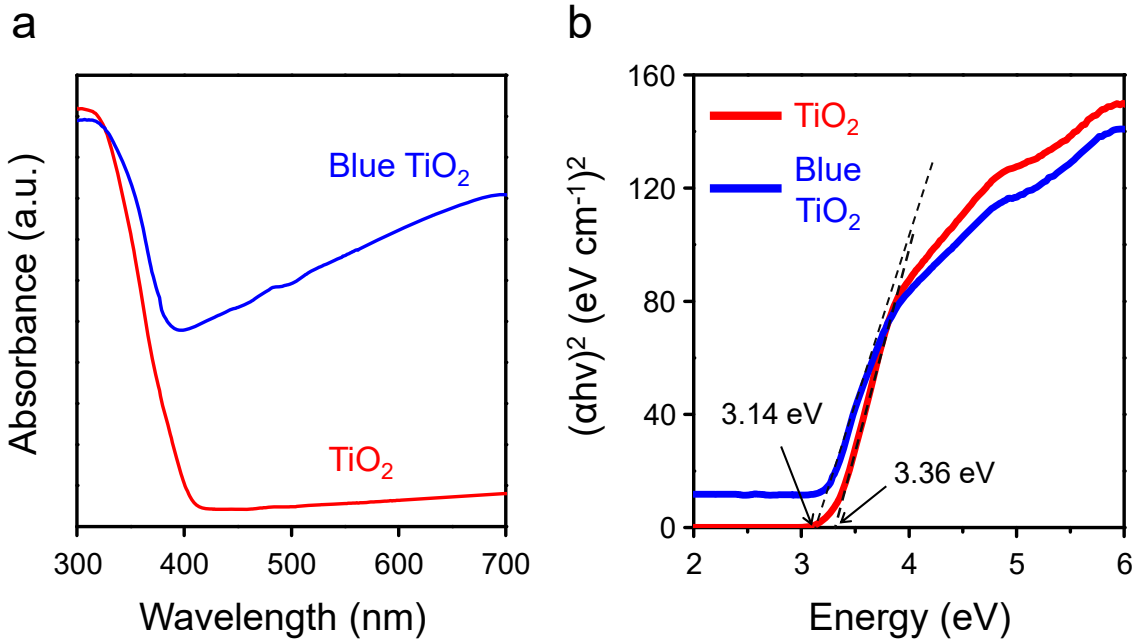

Fig. S2 (a) UV-Vis absorption spectra of TiO_2 and blue TiO_2 and (b) calculated band gap energy from UV-Vis absorption spectra.

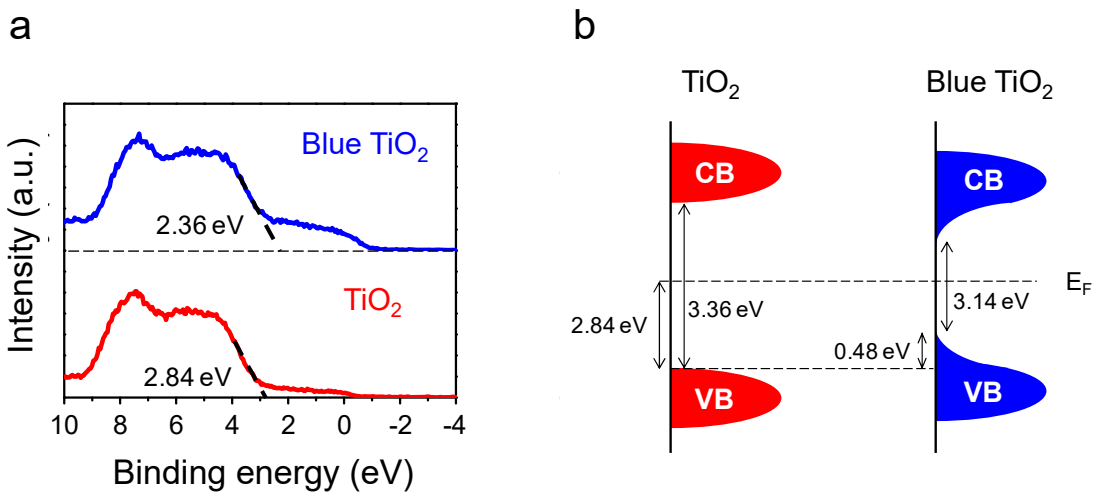

Fig. S3 (a) Valence band XPS spectra of TiO_2 and blue TiO_2 and (b) calculated bandgap scheme.

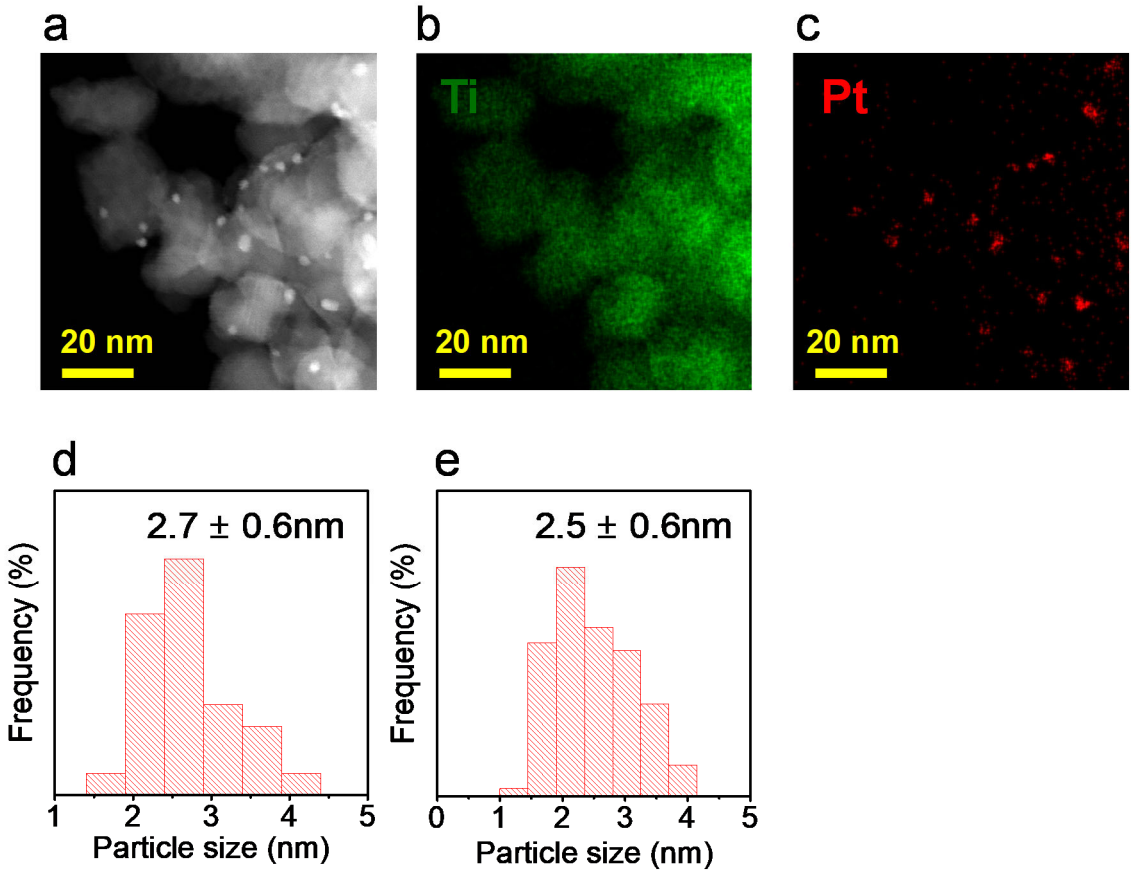

Fig. S4 (a) High-angle annular dark-field-scanning transmission electron microscopy (HAADF-STEM) image of Pt/blue TiO_2 and corresponding energy-dispersive X-ray spectroscopy (EDS) elemental mapping of (b) Ti, and (c) Pt. Particle size distribution of Pt nanoparticles on (d) TiO_2 and (e) blue TiO_2 before reaction.

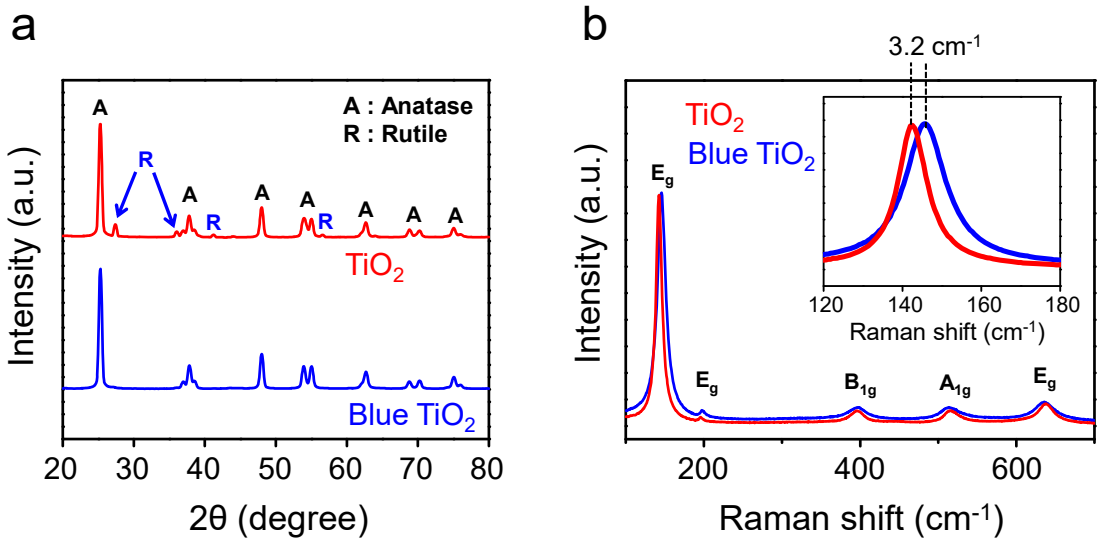

Fig. S5 (a) XRD pattern of TiO_2 and blue TiO_2. (b) Raman spectra of TiO_2 and blue TiO_2 and the inset is a magnification of the main peak located at 120-180 cm^{-1}.

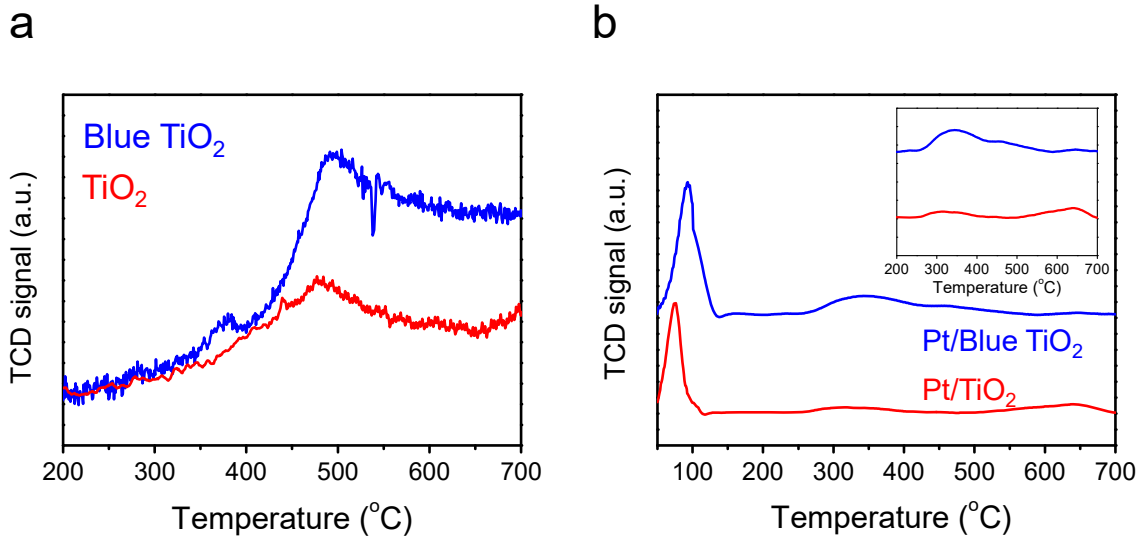

Fig. S6 H_2-TPR results of (a) TiO_2 and blue TiO_2 supports, and (b) Pt deposited on both supports.

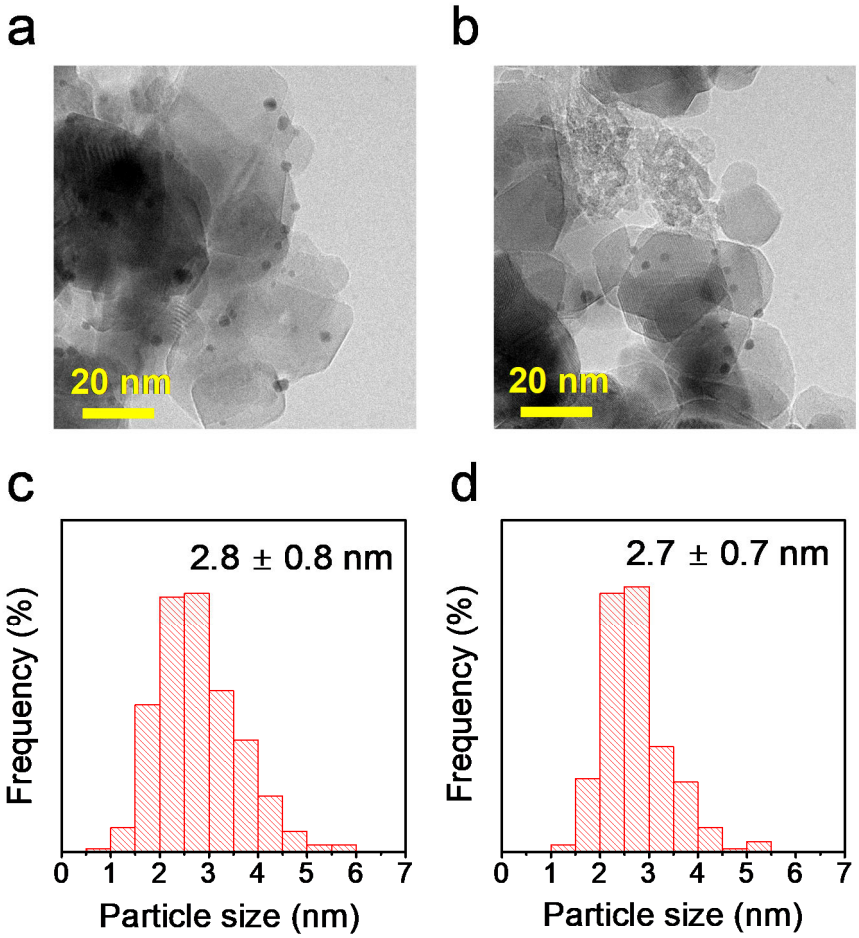

Fig. S7 TEM image of (a) Pt/TiO_2 and (b) Pt/blue TiO_2 after CO oxidation reaction. The particle size distribution of Pt nanoparticles of (c) Pt/TiO_2 and (d) Pt/blue TiO_2 after the reaction.

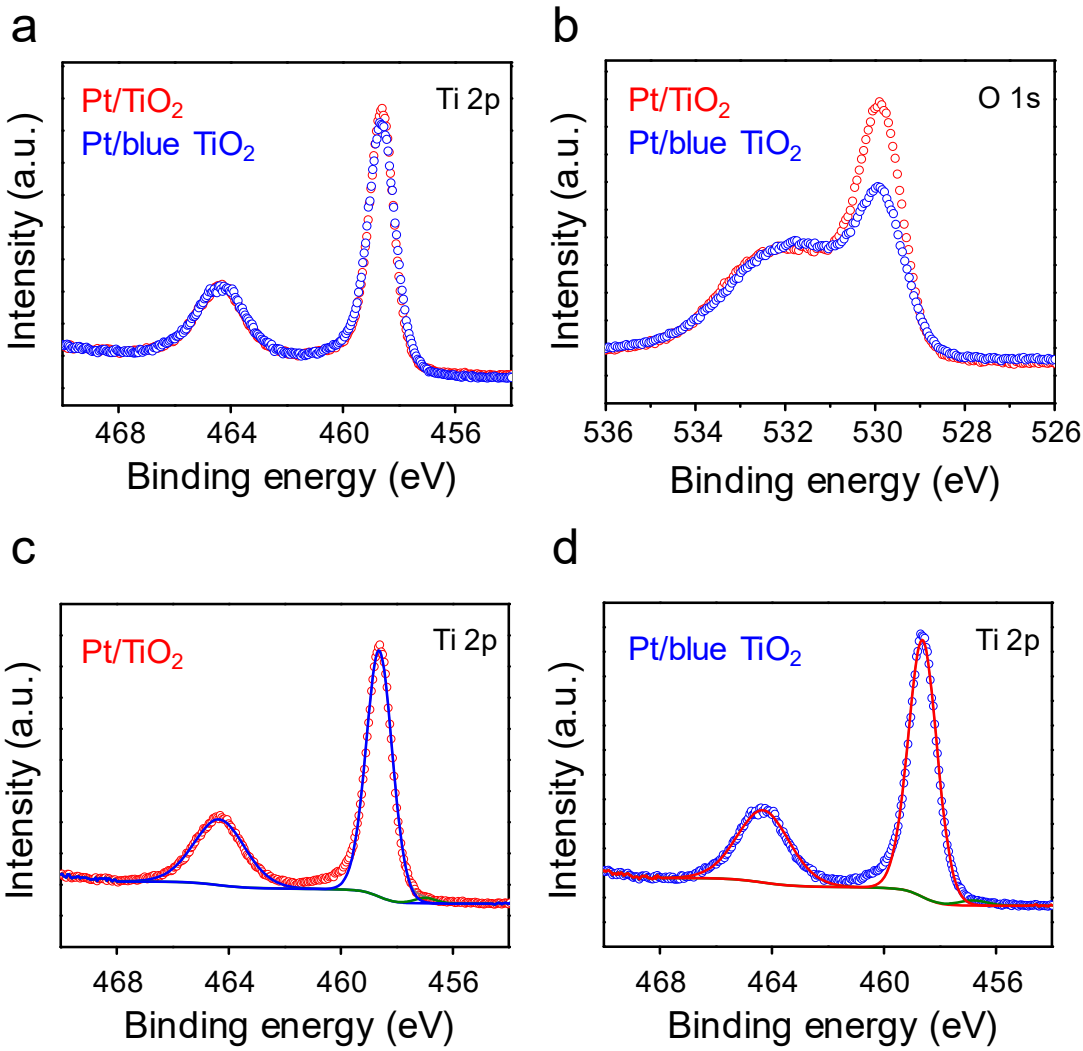

Fig. S8 (a) Ti 2p, and (b) O 1s XPS spectra of Pt/TiO_2 and Pt/blue TiO_2 after the CO oxidation reaction. Deconvolution of Ti 2p spectra of (c) Pt/TiO_2 and (d) Pt/blue TiO_2.

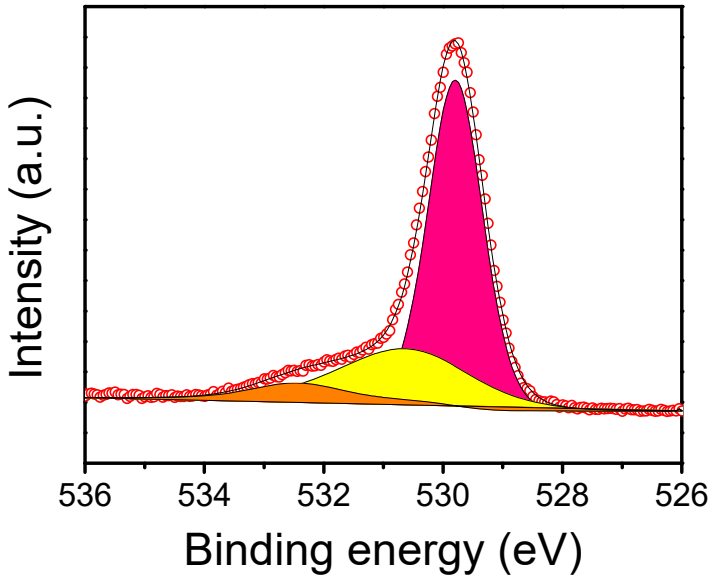

Fig. S9 Deconvolution of O 1s XPS spectra for Pt/TiO_2 catalysts before CO oxidation reaction.

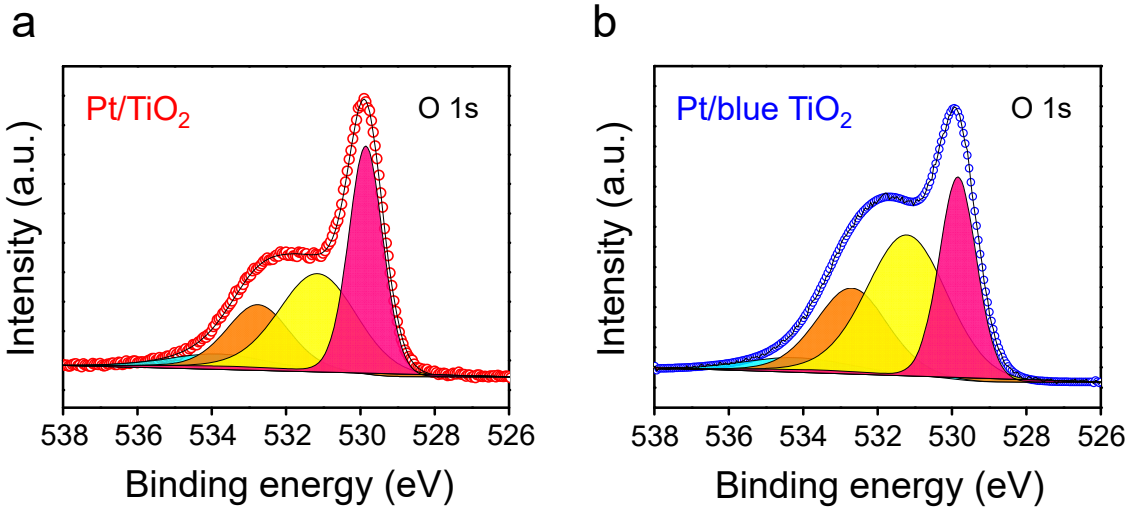

Fig. S10 (a) O 1s XPS spectra of Pt/TiO_2 and (b) Pt/blue TiO_2 catalysts after the CO oxidation reaction.

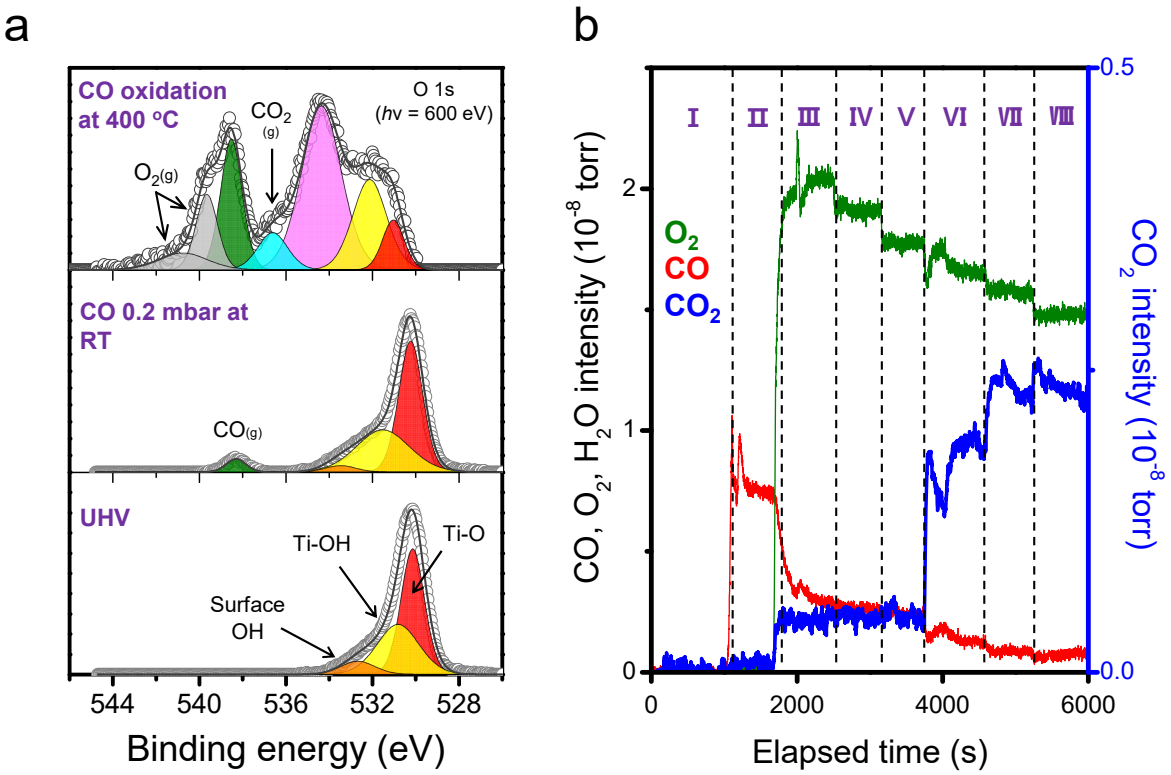

Fig. S11 (a) O 1s NAP-XPS spectra (*h*v = 600 eV) of Pt/TiO_2 under UHV, CO adsorption, and CO oxidation conditions. (b) Corresponding mass spectrometry spectra measured during the CO adsorption and oxidation; I: UHV, II: CO adsorption (0.2 mbar) at room temperature, III: CO oxidation (0.2 mbar of CO, and 0.5 mbar of O_2) at room temperature, CO oxidation at IV: 100 °C, V: 200 °C, VI: 250 °C, VII: 300 °C, VIII: 400 °C.

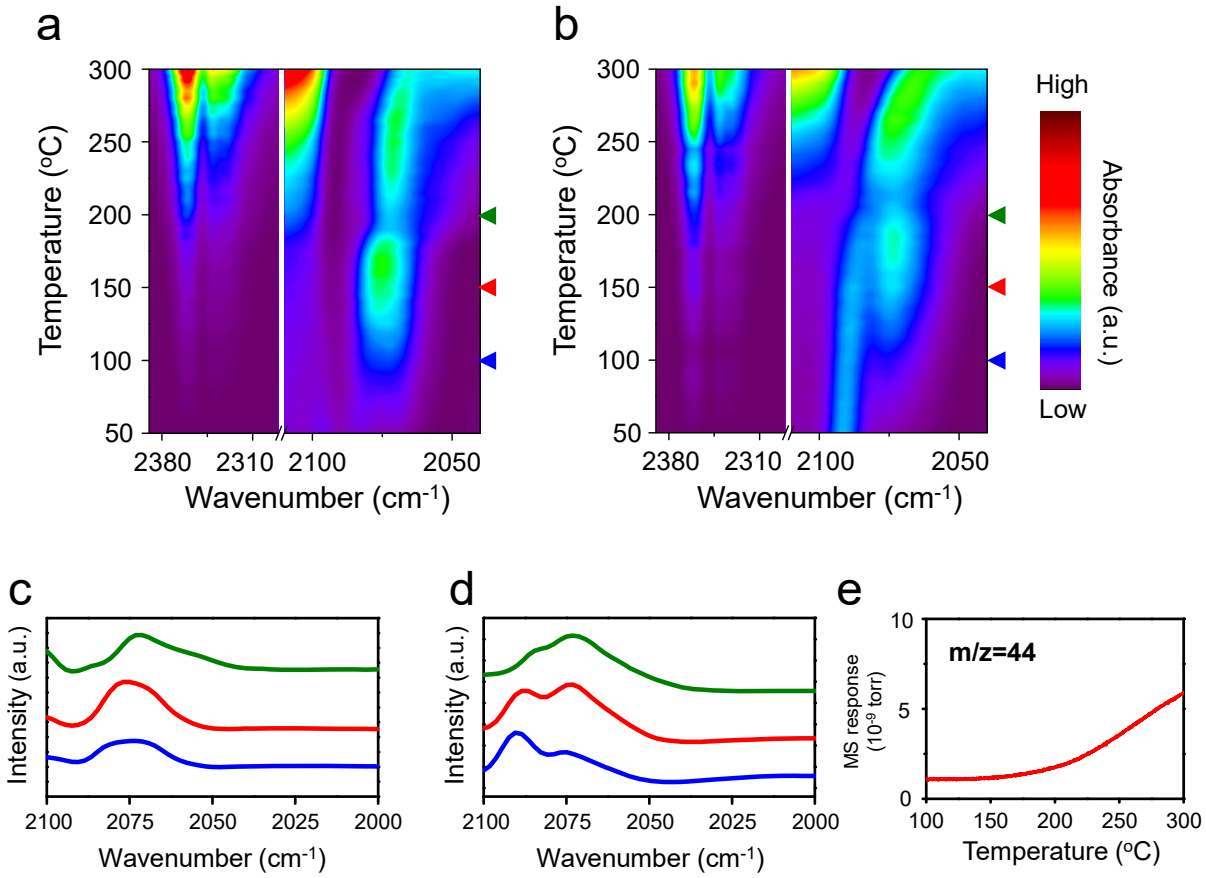

Fig. S12 In situ DRIFT contour image of (a) Pt/TiO_2 and (b) Pt/blue TiO_2 under CO flow (10 % CO/He) at elevated temperature. (b), and (d) DRIFT spectra at the temperature pointed by a triangle (100, 150, 200 °C) in contour map in (a), and (b), respectively. (e) CO_2 signal measured by MS under CO flow with Pt/blue TiO_2.

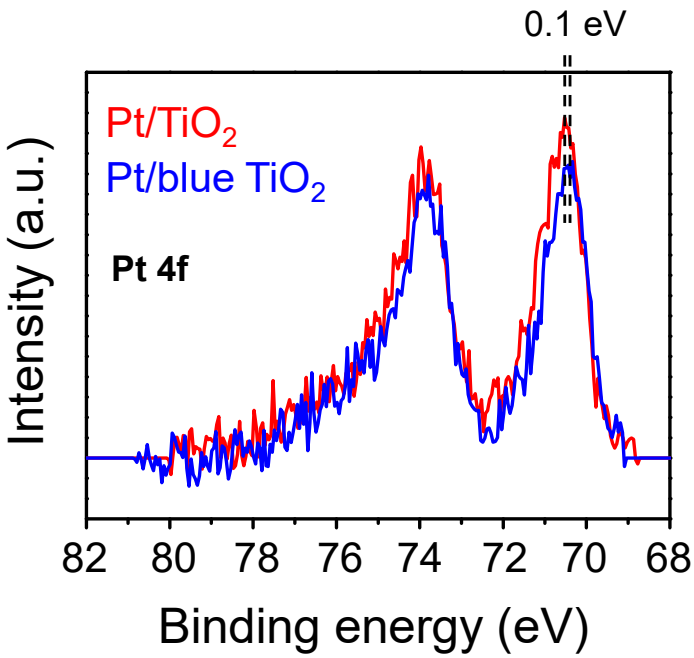

Fig. S13 Pt 4f XPS spectra with Pt/TiO_2 and Pt/blue TiO_2 catalysts before CO oxidation reaction.

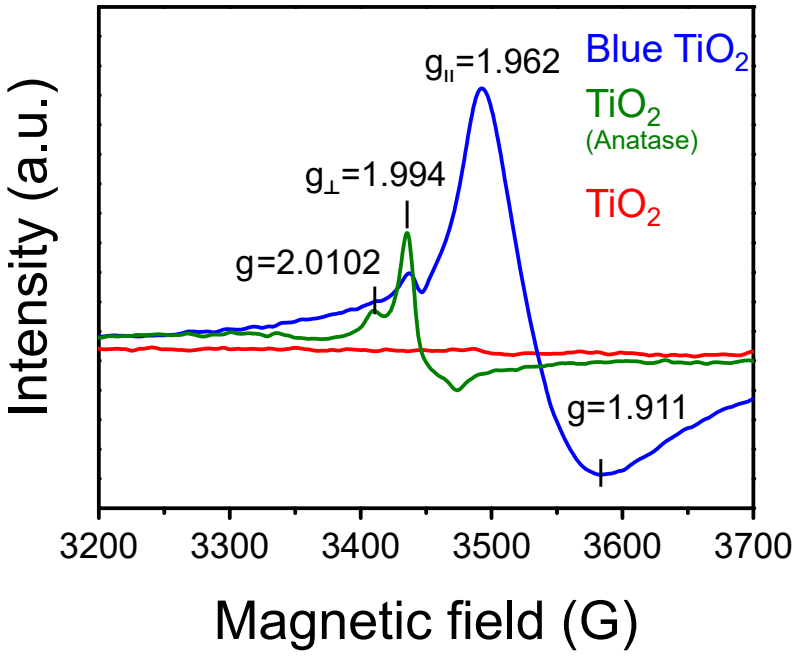

Fig. S14 EPR spectra of blue TiO_2 (blue line), TiO_2 (P25, red line), and TiO_2 (Anatase phase (Sigma Aldrich), green line). The spectra were collected at 77 K.